



POLITECNICO
MILANO 1863

**SCUOLA DI INGEGNERIA INDUSTRIALE
E DELL'INFORMAZIONE**

PROJECT REPORT - AERODYNAMICS OF TRANSPORT VEHICLES

Aerodynamic analysis of car boxes

Author: DANIELE TERRANEO, GIORGIO PACCHIONE, MARCO MADDONINI, PAOLO SARTI

Professors: PROF. ALEX ZANOTTI, PROF. PAOLO SCHITO

Assistant professor: ING. STEFANO NEGRI

Academic year: 2024-2025

1. Introduction

Aerodynamic performance is a critical factor in vehicles design, directly influencing fuel efficiency, stability, and external noise. When a box is mounted on a car, it introduces significant changes in airflow patterns, leading to increased drag and fuel consumption. For a generic vehicle, the drag force is determined by the frontal area A_f and by its shape, the aerodynamic quality of which is characterized by the drag coefficient C_D . The goal of the project is to investigate the aerodynamic performance of an Audi A4 Sedan equipped with different types of boxes and compare them using CFD simulations performed with *OpenFOAM*®. The analysis focuses on evaluating the drag and flow behaviour for several configurations, including variations in shape, dimension (long and wide boxes), mounting orientation (straight, reverse, and back boxes), and the addition of a spoiler on the car windshield, in front of the box. The results aim to identify the best designs and configurations to minimize drag and improve aerodynamic efficiency in order to save fuel.

2. Methodology

2.1. Car geometry

The CAD model of the car is taken from online resources [1], while the racks and boxes are

modeled using *PTC Creo Parametric*®. Careful attention is given to ensuring that all the boxes maintain the same volume throughout the modeling process. The wheels are approximated as cylinders with rounded-off edges and the car underbody is simplified as a smooth flat surface, in order to reduce the computational costs of the numerical simulations. The models are shaped and analyzed adopting a 1:1 scale, specifically with car dimensions of 4.7 m x 1.45 m x 1.98 m. Different boxes, shown in Figure 1, are modeled:

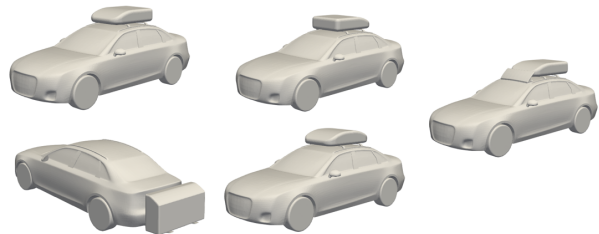


Figure 1: Box models

- A. Straight: the roof box is mounted in its typical forward-facing position;
- B. Reverse: the roof box is mounted in an unconventional reversed orientation;
- C. Back: the box is positioned further back on the roof, close to the rear windshield;
- D. Double curvature: the box has a double curvature on the front and rear part;

- E. Use of a spoiler placed in front of the roof box (straight configuration) to deflect air-flow.

2.2. Numerical setup

The CFD simulations are conducted in *OpenFOAM®*, using the stationary and incompressible solver simpleFoam. Furthermore, to reduce computational cost, a boundary condition of symmetry is enforced in the longitudinal plane $z = 0$. RANS incompressible simulations are performed and $k - \omega$ SST is chosen to model turbulence. Since the study relates to the aerodynamics of the car and the roof box, the inlet flow velocity is set to $30 \frac{\text{m}}{\text{s}}$ ($108 \frac{\text{km}}{\text{h}}$), which is a typical mean average speed on the highway. The ground boundary is modeled as a wall, moving at the stream velocity. However, wheel rotation is not considered in the analysis, since it is not the principal goal of the project and in order to save some computational efforts. The front and lateral walls of the domain are modeled as slip walls, while the back face is modeled as a pressure outlet at $p = 0 \frac{\text{m}^2}{\text{s}^2}$.

2.3. Mesh generation

Because of the symmetry of the geometry, half of the domain is considered allowing for a reduction in time and computational resources, even if this simplification is not representative of the flow in the entire domain but it is acceptable when the average of the forces is calculated. A farfield domain of $45 \text{ m} \times 9 \text{ m} \times 9 \text{ m}$, visible in Figure 2, is chosen in order to represent the open air condition and avoid boundary effects.

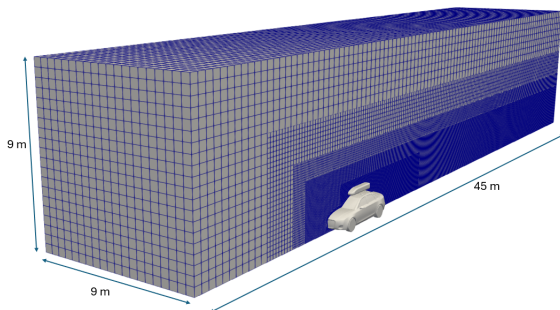


Figure 2: Mesh domain

This allows to have a good flow development above and beside the car, in the wake region. The mesh is generated using blockMesh and snappyHexMesh dictionaries in *OpenFOAM®*.

The external block is composed by four refinement boxes from level 1 to level 4 to guarantee a smooth decrease in cell dimension, as shown in Figure 3.

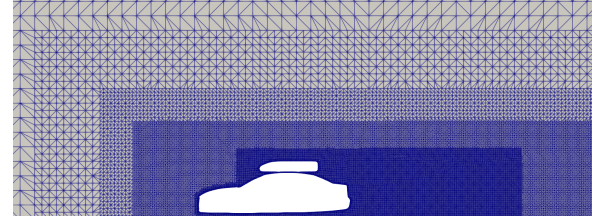


Figure 3: Refinement regions

The mesh is then pushed to a level 5 refinement upon the car. Finally, 5 layers with 1.1 expansion ratio are added (Figure 4) setting a first cell height such to retrieve a $30 < y^+ < 300$, large enough to satisfy the wall functions condition. This is done to better capture the higher gradients close to the car and critical zones such as around the box.

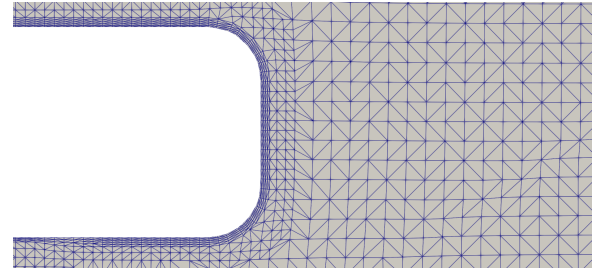


Figure 4: Inflate layers around the box

2.4. Grid convergence analysis

Grid convergence analysis is performed with three different meshes, by refining the blockMesh dictionary file increasing the number of cells in x , y and z directions. This is done to check the independence of the drag coefficient with respect to the number of cells and to select a mesh with a sufficient level of accuracy for the solution. In Table 1 are reported the three meshes used for the convergence study and the related parameters: the number of cells in each direction, the dimension of the single cell and the total number of elements.

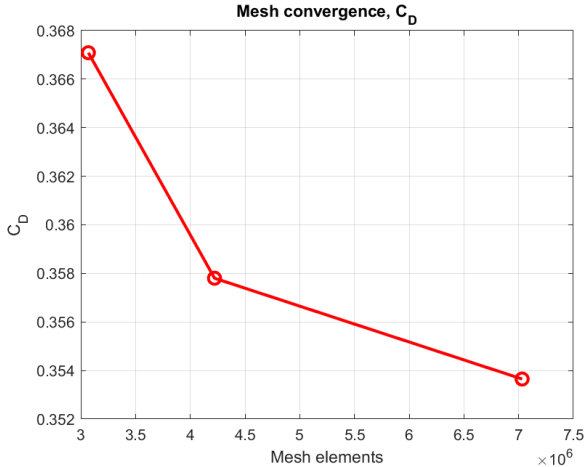
Lv0 is the dimension of the cell in the external block and it is the only parameter changed for the convergence analysis.

It is decided to use the medium mesh, for all cases studied, which represents a good compromise between mesh quality and computational

Type	x, y, z	Lv0	Cells
Coarse	(90 18 18)	0.5 m	3'068'987
Medium	(100 20 20)	0.45 m	4'221'399
Fine	(120 24 24)	0.375 m	7'031'907

Table 1: Meshes

time cost. By plotting the obtained drag coefficient with respect to the number of cells, the percentage variation of drag is calculated. It is shown in Figure 5 how the variation of C_D is halved passing from coarse to fine mesh. In fact, the relative ΔC_D passes from 2.53 % up to 1.16 % which is a reasonable value for the mesh independence. Moreover, the choice of using the medium mesh is justified by the goal of this project, which is understanding the relative drag benefits with different box configurations with respect to the car without any box.

Figure 5: Grid convergence, C_D

Due to computational limits, analyzing a mesh with more cells was unfeasible, but it is expected to eventually obtain a smaller decrease in the ΔC_D percentage variation.

2.5. Residuals and iterative convergence

In order to illustrate convergence, residuals of the simulation performed on the straight up box configuration are shown in Figure 6. 2000 iterations have been used for the simulations, showing a good behavior of the residuals.

The drag coefficient is also monitored providing a steady convergence solution as shown in Figure 7. Since some fluctuations are visible, an average on the C_D has been performed over the

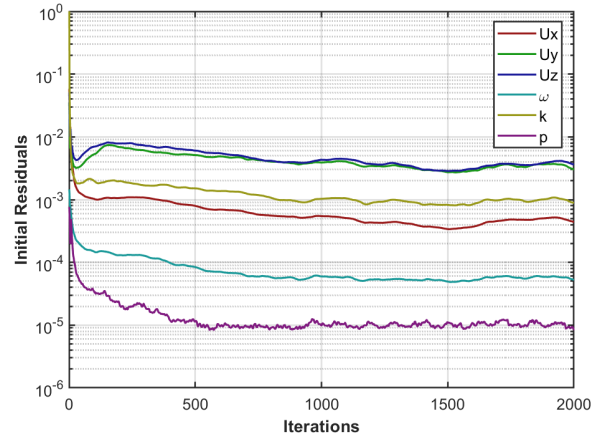


Figure 6: Residuals plot

last 500 iterations. The standard deviation σ is 0.0029, confirming a stable and convergent solution.

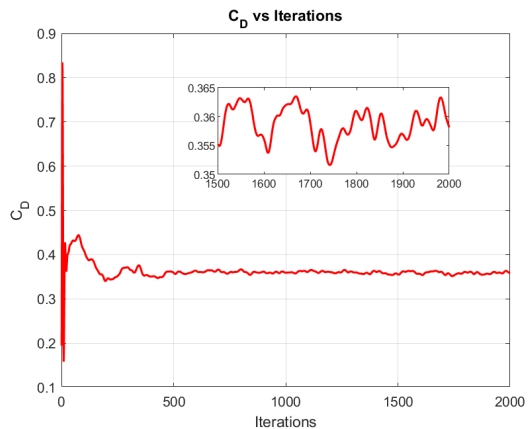


Figure 7: Drag coefficient plot

3. Results

In this section, the results obtained from the simulations in *OpenFOAM®* are presented. Specifically, the drag coefficients of both the long boxes (hereafter referred to as "long boxes") and the wide boxes (hereafter referred to as "wide boxes") are analyzed with respect to the car without any box. This will help to determine the most efficient configuration for studying fuel consumptions. Subsequently, the flow in different cases is examined, analyzing and comparing the pressure coefficients, dimensionless velocities, wakes and vortices in critical areas of interest.

3.1. Drag coefficient comparison

Once the simulations are performed, the results can be compared to see which is the best configuration. Since the aerodynamic resistance depends both on the C_D and on the frontal area, these two parameters are taken into account. In fact, the fuel consumption is determined by their product, given a certain dynamic pressure. In Table 2 a comparison between different set-ups is shown, also in terms of percentage increment of the C_D with respect to the baseline configuration. This refers to the case without any box. For an initial validation, the obtained drag coefficient of the baseline configuration was compared with the actual value of 0.27 declared by Audi [2]. It appears that the coefficient is slightly higher, which could be due to the fact that the rotation of the wheels was not considered.

Configuration	C_D	A_f [m^2]	ΔC_D
Baseline	0,3098	2,18	-
Long straight	0,3578	2,36	15,49 %
Long reverse	0,3701	2,36	19,46 %
Back	0,3244	2,18	4,71 %
Wide straight	0,3708	2,45	19,69 %
Wide straight, spoiler	0,3512	2,45	13,36 %
Wide double curvature	0,3506	2,45	13,04 %

Table 2: Drag coefficient results

In general, the best box mounting is the back one, which leads to an increase in drag of only 4.71 %. Hence, this solution happens to be the best for C_D value, the windward area, and the availability of space within the box. In fact, having the box in the back of the car reduces significantly the frontal area and consequently the drag.

Among the two long upper configurations, the best is the one in the straight direction, which results in a better C_D by 3.3 % compared with the reverse one.

The results also show that the implementation of a double curvature box leads to a quite significant improvement with respect to the wide straight box. Additionally, the implementation of a spoiler in the wide straight box leads to an actual improvement in terms of performances.

The phenomenology that leads to these results will be deeply analyzed in the following sections, where the software *ParaView*® was used to visualize the flow field in the different

configurations.

3.2. Long and back boxes

A post-processing analysis using *ParaView*® is performed to study the differences between the various box configurations simulated in *OpenFOAM*®. This allows for a physical justification of why one configuration is more efficient than another in terms of drag coefficient. Specifically, the configurations of the long boxes (straight, reverse and back) are now evaluated. The symmetry hypothesis must be considered as an approximation when analyzing the flow, since in reality the flow might not be symmetric. The pressure coefficient C_p is calculated as:

$$C_p = \frac{(p - p_\infty)}{\frac{1}{2} \rho_\infty V_\infty^2} \quad (1)$$

where $p_\infty = 0$ for incompressible simulations and p is the relative pressure.

In Figure 8 the different distribution of the pressure coefficient on the car can be observed. In all cases the front stagnation point is noticeable, characterized by a high pressure accumulation, where C_p reaches its maximum value.

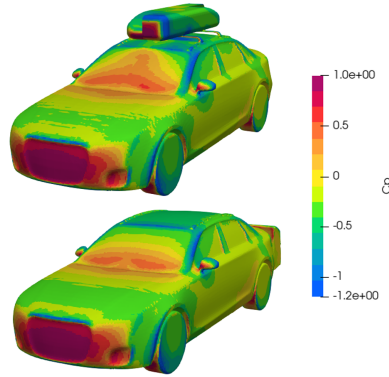


Figure 8: Pressure coefficient on long boxes

Additionally, in the straight and reverse configurations, the stagnation points generated by the frontal area of the boxes are clearly visible, with the reverse configuration showing a bigger area of high pressure. The presence of a negative pressure coefficient zone around the front-upper edges of the reverse box suggests that there may be a separation bubble with a greater detachment of vortices with respect to the straight box configuration. This may explain the increased

drag coefficient in the reverse set up. Moreover, it can be observed how the presence of the upper boxes influences the flow on the front windshield, which is characterized by a higher pressure value compared to the case with the rear box. From this image, it can be concluded that the position of the box directly affects the pressure distribution, primarily in the front and upper areas of the car. With the upper boxes, recirculation is greater near the roof, while with the rear box the disturbance shifts towards the rear region of the vehicle, remaining contained.

The dimensionless velocity fields in the three configurations show significant variations in the wake and flow separation phenomena depending on the box geometry. As visible in Figure 9, the acceleration of the flow over the sharp edge of the reverse box causes pronounced separations on the rear wall. Recirculation bubbles are more evident and extensive right after the sharp edge, differently from the straight box.

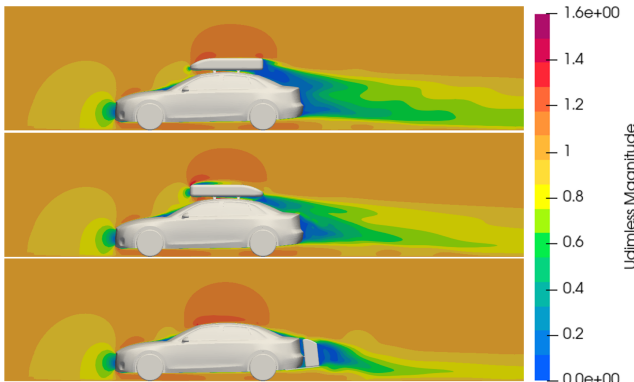


Figure 9: $U_{dimless}$ bidimensional field comparison of long straight, reverse and back boxes

These phenomena, even if the wake of the reverse configuration seems to be a little narrower, suggest a higher contribution to the aerodynamic drag.

In the back configuration, the absence of a box on the top of the vehicle keeps the flow more attached to the car's surface, with a smoother pressure gradient. The wake behind the back box, as shown in Figure 10, is confined to a narrower and more horizontally elongated area, suggesting less disturbance of the flow and, consequently, a reduction in drag with respect to the straight configuration.

The Q -criterion for the three configurations is visible in Figure 11. Q is defined as the second invariant of the velocity gradient tensor. Iso-

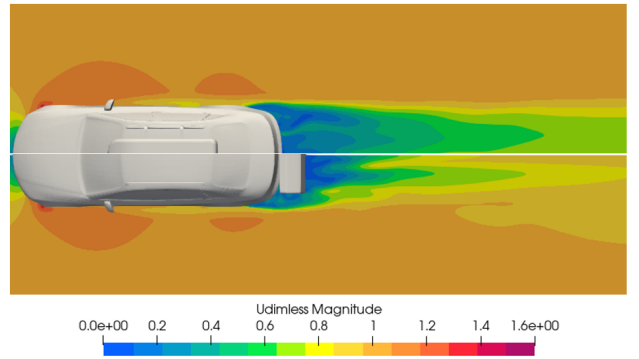


Figure 10: $U_{dimless}$ bidimensional field on a plane $z = 0.5$ m above the ground of long straight vs back box

surfaces of the Q -criterion help to understand the main vortical structures of the flow. This allows the identification of three-dimensional vortical structures, enabling the visualization of vortices and separation regions. In the upper box configurations, the flow separation is more abrupt: two vortices form at the rear edge of the box, increasing the wake thickness. The back box, instead, reduces the negative pressure in the wake due to a more gradual flow separation. Although the vortices are more numerous, they might be located in regions that minimize their negative impact on the overall drag. In both cases the longitudinal vortices generated from the C-pillar can be observed.

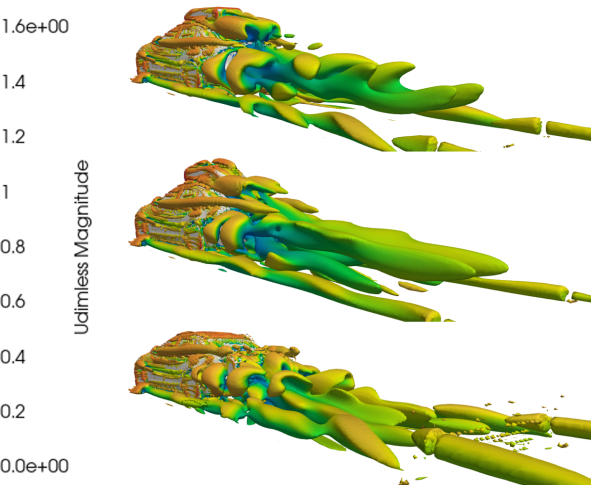


Figure 11: Q -criterion straight, reverse, back boxes

From this analysis, it can be concluded that the rear-mounted configuration is the most efficient in terms of wake reduction and vortex containment, resulting in a lower drag coefficient, as

derived from the simulations performed.

3.3. Wide vs long boxes

As mentioned in Section 1, the dimensions of the box were varied in length and width to potentially achieve aerodynamic improvement. The volume of the box was kept constant, but its width was increased while reducing its length. This adjustment was made to understand the effect of the frontal area on the drag. This also allowed for the subsequent implementation of a spoiler above the front windshield, for the wide box. The configurations of the long straight box versus the wide box are now compared to understand the differences in the flow fields. Also, the geometry of the double curvature box is analyzed. A comparison in pressure coefficient and adimensional velocity is taken into account.

The two wide boxes exhibit a more extensive high-pressure region due to their greater width, which has a negative effect in terms of drag coefficient. In the double curvature box, low-pressure areas can be observed across most of the surface, indicating a different distribution of aerodynamic forces. Figure 12 and Figure 13 show respectively the pressure coefficient and dimensionless velocity fields on the two-dimensional symmetry cross-section.

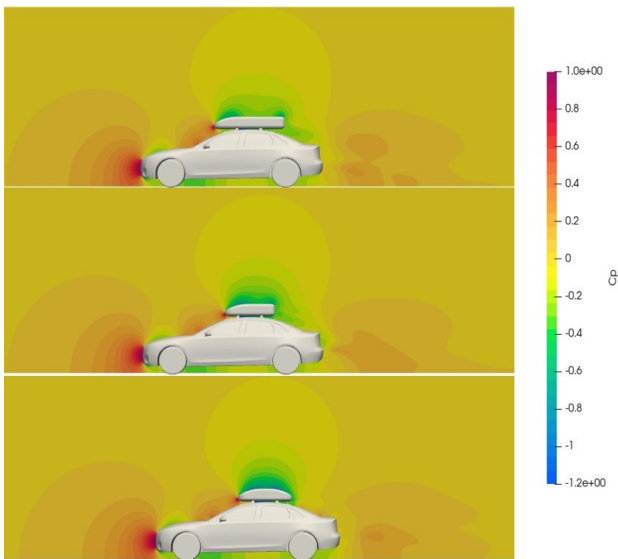


Figure 12: C_p bidimensional field comparison of long, wide and double curvature boxes

The two straight configurations exhibit comparable pressure and velocity fields on the symmetry plane. The box with double curvature, on the other hand, shows a low-pressure area

across the entire surface that allows for pressure recovery over the rear section of the car, which is therefore higher compared to the other two configurations. This generates a smaller wake. Looking at Figure 14 it is possible to observe how the curvature in the third case allows the flow to follow the contour closely, preventing the separation that characterizes the other two configurations. A slice of the boxes is taken at an height of 1.6 m above the ground, showing clearly how the wake of the second configuration is actually wider, leading to poorer performance. For the double curvature, the wake is shorter and more compact compared to the second configuration. The double curvature indeed promotes a more controlled flow separation, reducing the size of the wake.

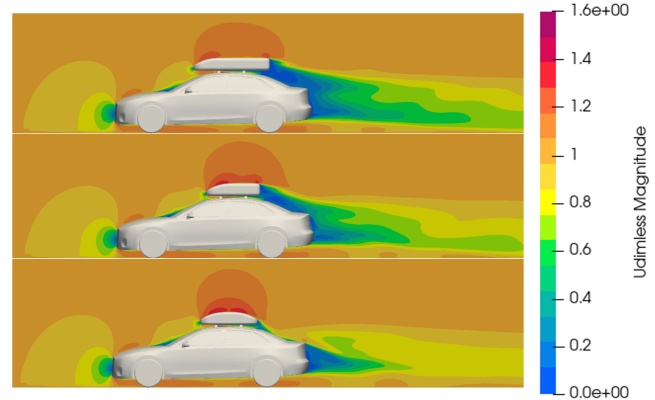


Figure 13: $U_{dimless}$ field comparison of long, wide and double curvature boxes

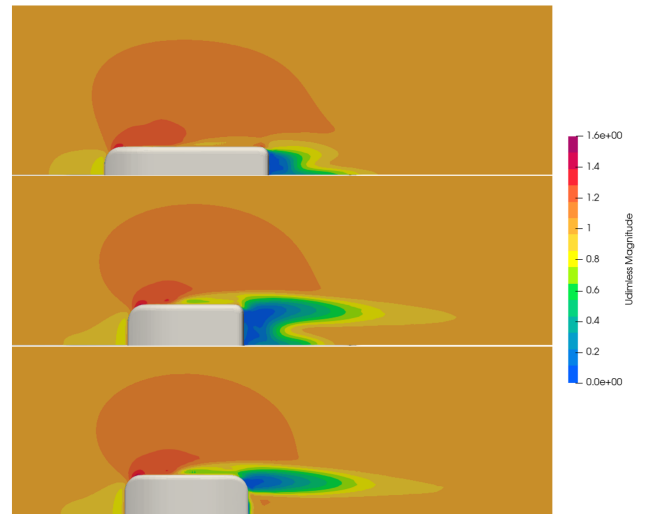


Figure 14: $U_{dimless}$ slice at $z = 1.6$ m comparison of long, wide and double curvature boxes

Overall, the configuration with the wide straight

box proves to be the worst in terms of drag. The other two setups, however, exhibit comparable C_D values, as the narrower wake produced by the double curvature design is offset by its larger frontal area, nearly canceling out the benefits with respect to the long straight box.

3.4. Spoiler Implementation

As a final point, the effect of introducing a spoiler on the aerodynamic performance of the vehicle with an upper wide box is investigated. Particularly significant in this regard is the comparison of the straight configuration with and without a spoiler. In Table 3 the results of the two simulations can be observed. The use of the spoiler achieves a drag reduction of 5.2 %.

Configuration	C_D	ΔC_D
Wide straight	0.3708	-
Wide straight, spoiler	0.3512	-5.2 %

Table 3: C_D comparison between the straight wide box configuration with and without the spoiler

The difference in drag can be explained by examining the Figure 15, which shows the difference in terms of C_p between the two configurations. It is noticeable that the configuration without the spoiler exhibits a higher C_p peak at the front of the box. This results in an increase in drag compared to the one with the spoiler, which is instead characterized by a less pronounced pressure peak at the spoiler's location, due to the flow deflection.

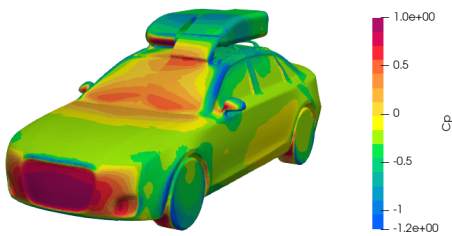


Figure 15: C_p comparison between the straight wide box configuration with and without the spoiler

In Figure 16 the wake generated by the two configurations is shown. It can be observed that, without the spoiler, the wake is wider, indicating a more pronounced flow separation. This generates larger vortices and greater pressure drag.

With the spoiler, on the other hand, the wake is narrower and more confined, suggesting a more orderly flow.

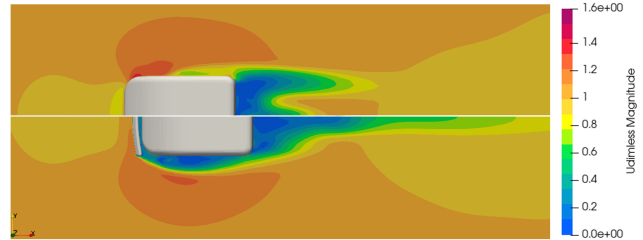


Figure 16: $U_{dimless}$ slice at $z = 1.6$ m comparison of wide straight box with and without the spoiler

Vortical structures can be visualized with the Q – criterion in Figure 17. The vortices behind the box and the vehicle are clearly visible. The spoiler modifies the flow leading to a smaller separation and to smaller vortices behind the box. Finally, it can be stated that, based on the analysis conducted, using a spoiler is better than having a longer and narrower box.



Figure 17: Q -criterion for the wide box with and without the spoiler

3.5. Fuel consumption

Once it has been observed that the presence of storage boxes on the roof or at the rear of the vehicle leads to a significant increase in the drag coefficient (and of course on the windward area), it becomes interesting to examine how this increase in drag affects the vehicle's everyday use. The most relevant parameter to analyze is undoubtedly fuel consumption. Starting from an estimation of the total force resistance to mo-

tion, the following equation can be used:

$$F_t = F_r + F_w = m g C_r + \frac{C_D A_f \rho V_\infty^2}{2} \quad (2)$$

where F_r is the rolling resistance, F_w is the aerodynamic resistance, C_r is the rolling resistance coefficient, A_f is the windward area and m is the vehicle mass.

The speed chosen for the consumption analysis is $V_\infty = 30 \frac{\text{m}}{\text{s}}$, which corresponds to the speed used in the simulations and could represent the average cruising speed of a vehicle on a highway. For this velocity, a reasonable value for C_r is 0.013 [3]. In the previous formula, the total force resistance F_t depends on the rolling resistance of the tires and the aerodynamic drag. To perform a more accurate analysis, it would be necessary to have not only aerodynamic data but also information about the engine, tires and wheels. Moreover, fuel consumption also depends on the conditions under which the vehicle operates, such as traffic and weather conditions. It is possible to calculate the average required power as:

$$P_t = F_t V_\infty \quad (3)$$

and the energy required as:

$$E_t = P_t t = P_t \frac{S}{V_\infty} \quad (4)$$

For the energy calculation, it is assumed that the required power E_t remains constant throughout the entire distance traveled S , assumed to be 200 km, even if the fuel consumption leads to a decrease in the total mass, hence a decrease in the rolling resistance.

Finally, the amount of fuel in liters (V_{fuel}) and the consumption (C in $\frac{\text{Km}}{\text{l}}$) are given by the formulas:

$$V_{fuel} = \frac{E_t}{\eta H \rho_{fuel}} \quad (5)$$

$$C = \frac{S}{V_{fuel}} \quad (6)$$

In the previous equation, $H = 43.953 \frac{\text{MJ}}{\text{Kg}}$ represents the calorific value of gasoline [4], $\rho_{fuel} = 0.7 \frac{\text{Kg}}{\text{l}}$ is the density of gasoline at an ambient temperature, and for the efficiency of the thermal gasoline engine it can be assumed $\eta = 0.3$. The Figure 18 shows the fuel consumption of the various configurations and the Table 4 shows the variation of consumption.

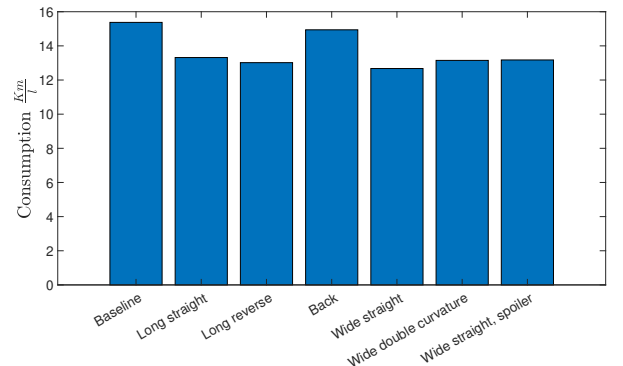


Figure 18: Bar chart showing the fuel consumption of different setups

Configuration	ΔC
Baseline	-
Long straight	-13.39 %
Long reverse	-15.34 %
Back	-2.83 %
Wide straight	-17.57 %
Wide double curvature	-14.47 %
Wide straight, spoiler	-14.31 %

Table 4: Fuel consumption variation of the different setups with respect to the baseline

4. Wind tunnel test

4.1. Set up

In order to validate the results obtained by the CFD, the model was 3D printed and tested in a wind tunnel where the stream can reach a maximum speed of $20 \frac{\text{m}}{\text{s}}$ and it is powered by a 2.2 kW motor which supplies a single-stage axial fan in order to generate the unidirectional air flow. The test section is a 1000 mm x 500 mm x 500 mm box with lateral entrances to allow the positioning of the model and supplied with a load balance to measure the forces and moments along the three main directions. The model was scaled by a factor of 1:15. Only the most relevant cases were tested, hence, the baseline, the straight long box, the reverse long box (presented in Figure 19) and the back box. The laboratory set up was made up of a Pitot tube, a 6 components balance and the software to record the data and the inverter to regulate the fan power.

The model was excavated at the center, in order to make it possible for the balance to be inside the model. The value of the velocity

used for the tests was obtained from the Pitot tube, which provides a measure of the dynamic pressure after the convergent duct, through the following relation:

$$V_\infty = \sqrt{\frac{2 p_{dyn}}{\rho}} \quad (7)$$



Figure 19: 3D car model in wind tunnel

In order to avoid the influence of the model on the read of the Pitot tube, the reading from the Pitot tube was taken without the model in the test section at a certain power output from the fan. Different power settings were tested on various test days, resulting in dynamic pressures of 50 Pa, 100 Pa, 150 Pa and 200 Pa. In any case, the tests carried out provided similar values. Only the results at 100 Pa, corresponding to a velocity of $12.78 \frac{m}{s}$ were reported, as they were considered the most reliable because the force values obtained at higher and lower power settings showed greater fluctuations and exhibited more noise. This power output remained constant throughout all the tests, just switching on and off the fan. The data have been acquired for 10 s with a sample rate of 125 Hz.

To prevent interference with the tunnel boundary layer, the model was elevated from the lower wall of the tunnel.

4.2. Results

The data have been averaged and filtered to get more reliable results, eliminating the contribution of the noise generated by the vibrations induced by the fan.

The force values obtained during the experimental test are shown in the Table 5.

Configuration	F_x
Baseline	0.4880 N
Long straight	0.5441 N
Long reverse	0.5442 N
Back	0.4903 N

Table 5: Force values for different configurations

Particular attention was given to the evaluation of additional drag components. Specifically, the drag contribution of the supports holding the model was calculated. For this purpose, the tare effects of the supports were determined through a dedicated experimental test and subtracted from the obtained drag. For a more accurate assessment, it would be beneficial to evaluate interference effects as well but due to the geometry of the balance and the supports this was not possible. As can be seen in the Table 6, these additional drag components are far from being insignificant.

Type	F_x
Supports and plate	0.1808 N
Supports	0.0531 N

Table 6: Tare drag contributes

Since the plate was embedded in the model, the only effect considered was that of the supports. It is worth noting that, considering interference effects, the 'spurious' drag components would be even more significant in relation to the low aerodynamic forces acting on such a small model. Particular attention must be paid to the blockage effect. During wind tunnel tests, the walls restrict the flow field around the vehicle causing a flow acceleration and an increased measured drag. This can also influence the boundary layer and increment its thickness. For this reason, the blockage [5] must be taken into account:

$$B = 1 - 2.5 \frac{A_f}{A_t} \quad (8)$$

Where B is the blockage, A_f is the frontal area and A_t is the wind tunnel section area.

Taking into consideration the aforementioned corrections the drag coefficient is computed as:

$$C_{D_{exp}} = B \frac{F_x - F_{supports}}{\frac{1}{2} A_f \rho V_\infty^2} \quad (9)$$

Table 7 shows the drag coefficients obtained and their differences with respect to CFD.

Configuration	$C_{D_{exp}}$	$C_{D_{CFD}}$	ΔC_D
Baseline	0.3952	0.3098	27.57 %
Long straight	0.4091	0.3578	14.34 %
Long reverse	0.4092	0.3701	10.29 %
Back	0.3973	0.3244	22.46 %

Table 7: Drag comparison between experiments and CFD results

The wind tunnel simulation confirms the trend observed in the CFD results, with the back configuration proving to be the most effective, followed by the long straight and the long reverse configurations which give basically the same results. The relative differences are not preserved. This discrepancy may primarily be attributed to the imperfect assembly of the various boxes and, secondly, to potential inaccuracies caused by the balance, which should have been recalibrated. The comparison between the CFD and wind tunnel results reveals significant differences, primarily due to the aforementioned experimental errors related to the wind tunnel setup. Additionally, the discrepancies can be ascribed to the fact that the CFD simulations were conducted at a different Reynold's number, reproducing free stream conditions.

5. Conclusions

An analysis was conducted to evaluate the impact of car boxes on aerodynamic performance by examining the key aerodynamic phenomena involved. The results indicated that the frontal area of the boxes adversely affects aerodynamic efficiency, while the implementation of a spoiler can lead to performance improvements. The analysis identified the back box as the optimal solution in terms of aerodynamic efficiency. Furthermore, a consumption analysis was carried out to highlight the differences between various

configurations under real-world operating conditions. Finally, wind tunnel tests validated the findings obtained from numerical simulations, with observed discrepancies attributed to differences in Reynolds numbers and measurement conditions.

References

- [1] Grabcad, 2025. URL <https://grabcad.com/library>.
- [2] Audi a4 sedan drag coefficient. URL <https://www.audi-mediacenter.com/en>.
- [3] P.Schito A.Zanotti. Slides from the lectures of the course of aerodynamics of transport vehicles, A.Y. 2024/2025.
- [4] ENEA, 2025. URL <https://www.efficienzaenergetica.enea.it/>.
- [5] E.C.Maskell. *Theory of the blockage effects on bluff bodies and stalled wings in a closed wind tunnel*. Ministry of Aviation (UK), 1963.